Journal of Controlled Release 172 (2013) 823–831

Contents lists available at ScienceDirect

Journal of Controlled Release

journal homepage: www.elsevier.com/locate/jconrel

NANOMEDICINE

Enhanced drug-loading and therapeutic efficacy of hydrotropic oligomer-conjugated glycol chitosan nanoparticles for tumor-targeted paclitaxel delivery

Heebeom Koo [a,1], Kyung Hyun Min [a,b,1], Sang Cheon Lee [c], Jae Hyung Park [d], Kinam Park [e], Seo Young Jeong [b], Kuiwon Choi [a], Ick Chan Kwon [a,f,*], Kwangmeyung Kim [a,**]

[a] Center for Theragnosis, Biomedical Research Institute, Korea Institute of Science and Technology, 39-1 Hawolgok-dong, Seongbuk-gu, Seoul 136-791, Republic of Korea
[b] Department of Life and Nanopharmaceutical Science, Kyung Hee University, 1 Hoegi-dong, Dongdaemun-gu, Seoul 130-701, Republic of Korea
[c] Department of Maxillofacial Biomedical Engineering, School of Dentistry, Kyung Hee University, 1 Hoegi-dong, Dongdaemun-gu, Seoul 130-701, Republic of Korea
[d] Department of Polymer Science and Engineering, Sungkyunkwan University, Suwon 440-746, Republic of Korea
[e] Departments of Pharmaceutics and Biomedical Engineering, Purdue University, West Lafayette, IN 47907, USA
[f] KU-KIST School, Korea University, 1 Anam-dong, Seongbuk-gu, Seoul 136-701, Republic of Korea

ARTICLE INFO

Article history:
Received 17 June 2013
Accepted 22 August 2013
Available online 11 September 2013

Keywords:
Hydrotropic oligomer
Glycol chitosan nanoparticles
Tumor-targeting
Paclitaxel
Drug delivery
Cancer therapy

ABSTRACT

Enhanced drug-loading and therapeutic efficacies are highly essential properties for nanoparticles as tumor-targeting drug carriers. Herein, we developed the glycol chitosan nanoparticles with hydrotropic oligomers (HO-CNPs) as a new tumor targeting drug delivery system. For enhancing drug-loading efficiency of paclitaxel in drug carriers, hydrotropic 2-(4-(vinylbenzyloxy)-N,N-diethylnicotinamide) (VBODENA-COOH) oligomers, that were used for enhancing the aqueous solubility of paclitaxel, were directly conjugated to glycol chitosan polymers. The amphiphilic conjugates readily formed nanoparticle structure (average size = 302 ± 22 nm) in aqueous condition. Water-insoluble paclitaxel (PTX) was readily encapsulated into HO-CNPs with a high drug-loading amount up to 24.2 wt.% (2.4 fold higher than other polymeric nanoparticles) by a simple dialysis method. The PTX encapsulated HO-CNPs (PTX-HO-CNPs; average size = 343 ± 12 nm) were very stable in aqueous media up to 50 days. Also, PTX-HO-CNPs presented rapid cellular uptake and lower cytotoxicity in cell culture system, compared to Cremophor EL/ethanol formulation of PTX. In tumor-bearing mice, the extravasation and accumulation of PTX-HO-CNPs in tumor tissue were precisely observed by intravital fluorescence imaging techniques. Furthermore, PTX-HO-CNPs showed the higher therapeutic efficacy, compared to Abraxane®, a commercialized PTX-formulation. These overall results demonstrate its potential as a new nano-sized PTX carrier for cancer treatment.

© 2013 Elsevier B.V. All rights reserved.

1. Introduction

Nanoparticles have emerged as attractive materials in biomedical researches. They have showed great utility in many fields (imaging, drug delivery, gene delivery, etc.), and proved their potential with promising animal data in large amount of research papers [1–3]. They particularly showed two main advantages, compared to traditional formulation of water-insoluble anticancer drugs. First, they can solubilize hydrophobic anticancer drugs in aqueous condition without a toxic organic solvent or detergent. Nanoparticles such as liposomes or micelles have amphiphilic nanoparticle structures, so hydrophobic anticancer drugs could be easily encapsulated into these nanoparticles [4,5]. This ability enabled more convenient dissolution and injection of hydrophobic anticancer drugs for cancer therapy. Second, their targeting ability to the disease site like tumor tissues [6]. The nanometer size of nanoparticles is suitable for preventing renal clearance in kidney and long circulation in blood flow. Particularly, anticancer drug-encapsulated nanoparticles could easily penetrate the fenestrate blood vessels in angiogenic tumor site. Consequently, they have presented higher tumor tissue accumulation compared to natural anticancer drugs, which is denoted as the enhanced permeation and retention (EPR) effect [7].

Until now, many researchers have focused on the tumor-targeting efficiency of anticancer drug-encapsulated nanoparticles in various tumor-bearing animal models. They optimized the physicochemical properties of nanoparticles like their sizes or surface charges, and they conjugated some ligands that bind to the receptors on the target cell surface [2,8]. However, relatively fewer researchers to date focused on the degree of the solubilizing ability for hydrophobic anticancer drugs within nanoparticles, wherein the drug-loading efficiency of various

* Correspondence to: I.C. Kwon, KU-KIST School, Korea University, 1 Anam-dong, Seongbuk-gu, Seoul 136-701, Republic of Korea.
** Corresponding author.
E-mail addresses: ikwon@kist.re.kr (I.C. Kwon), kim@kist.re.kr (K. Kim).
[1] These authors contributed equally to this paper.

0168-3659/$ – see front matter © 2013 Elsevier B.V. All rights reserved.
http://dx.doi.org/10.1016/j.jconrel.2013.08.297

nanoparticles is mostly about10 wt.% in the nanoparticles [9,10]. If the required amount of nanoparticles is too high to solubilize small amounts of hydrophobic anticancer drugs, it will not be effective for commercialization, due to the high cost for preparing nanoparticle-based formulation. Some recent papers reported the long-term harmful effect of nanoparticles, which significantly demonstrate that researchers should pay more attention to the biocompatibility of nanoparticles for clinical application [11]. Therefore, the amount of nanoparticles is very important even though they showed negligible acute toxicity.

Paclitaxel (PTX) is one of the representative water-insoluble anticancer drugs, which quickly binds to and stabilizes microtubules, followed by inhibition of mitosis during cell division [12]. However, it has extremely poor water solubility (lower than about 1 μg/ml), which inhibits its direct application to human body. Consequently, special formulation using ethanol and Cremophor EL is required to solubilize PTX for intravenous injection, which is reported to result in harmful side effect such as neurotoxicity and hypersensitivity [13,14]. To overcome this problem, many researchers have tried to use hydrotropic agents which can enhance the water solubility of poorly soluble drugs at high concentration. For example, Park group found that N,N-diethylnicotinamide (DENA) derivatives were most effective hydrotropic agent to solubilize PTX [15]. Previously, we conjugated the hydrotropic DENA oligomer (HO) to glycol chitosan nanoparticles for increasing the PTX's loading amount up to 24 wt.% [16]. Furthermore, the PTX encapsulated HO-CNPs (PTX-HO-CNPs) efficiently decreased the cytotoxicity, compared to that of free PTX formulation dissolved in 50/50% Cremophor EL/ethanol mixture.

Herein, we optimized the glycol chitosan nanoparticles with hydrotropic oligomers (HO-CNPs) with higher loading amount and stability in aqueous condition (Scheme 1). The therapeutic efficacy of PTX-HO-CNPs was evaluated in tumor-bearing mice. The drug-loading efficiency, stability, and cellular uptake of PTX-HO-CNPs were carefully studied *in vitro*. Also, we analyzed the *in vivo* biodistribution of PTX-HO-CNPs in tumor-bearing mice after intravenous injection by optical imaging. We precisely observed PTX-HO-CNP's movement in blood vessels of tumor tissue by intravital imaging techniques. Finally, we evaluated its therapeutic efficacy *in vivo*, compared it to Abraxane®, commercialized formulation of PTX [17].

2. Materials and methods

2.1. Materials

Glycol chitosan (Mw = 2.5×10^5; degree of deacetylation = 82.7%) was purchased from Sigma (St. Louis, MO), purified by filtration, and dialyzed against deionized distilled water. [1-Ethyl-3-(dimethylamino) propyl]carbodiimide hydrochloride (EDAC), 4-vinylbenzyl chloride, 2-hydroxynicotinic acid, diethylamine, 3-mercaptopropionic acid (MPA), and anhydrous N,N-dimethylformamide were purchased from Sigma-Aldrich (St. Louis, MO). 1-Hydroxybenzotriazole (HOBt) was received from TCI (Tokyo, Japan). Paclitaxel was obtained from Samyang Genex Co. (Daejeon, Korea). N,N-Azobisisobutyronitrile (AIBN), purchased from Sigma-Aldrich, was purified by recrystallization in methanol. Abraxane® was obtained from Abraxis BioScience, LLC. (Los Angeles, U.S.A.). All other reagents used in the experiments were analytical grade and used as received. 2-(4-(vinylbenzyloxy)-N,N-diethylnicotinamide) (VBODENA) monomer was prepared as reported in previous paper [18].

2.2. Synthesis of hydrotropic oligomer-conjugated glycol chitosan nanoparticles (HO-CNPs)

Hydrotropic oligomer-conjugated glycol chitosan nanoparticles (HO-CNPs) were synthesized as reported previously [16]. In brief, hydrotropic VBODENA oligomers, oligo(VBODENA)-COOH, were synthesized by free radical chain transfer polymerization of VBODENA using MPA as a chain transfer agent and AIBN as an initiator. Then, it was conjugated to glycol chitosan polymer in the presence of EDAC and HOBT. Glycol chitosan (100 mg) was dissolved in distilled water (5 ml) and added to oligo(VBODENA)-COOH (67.03 mg) in methanol (5 ml). The

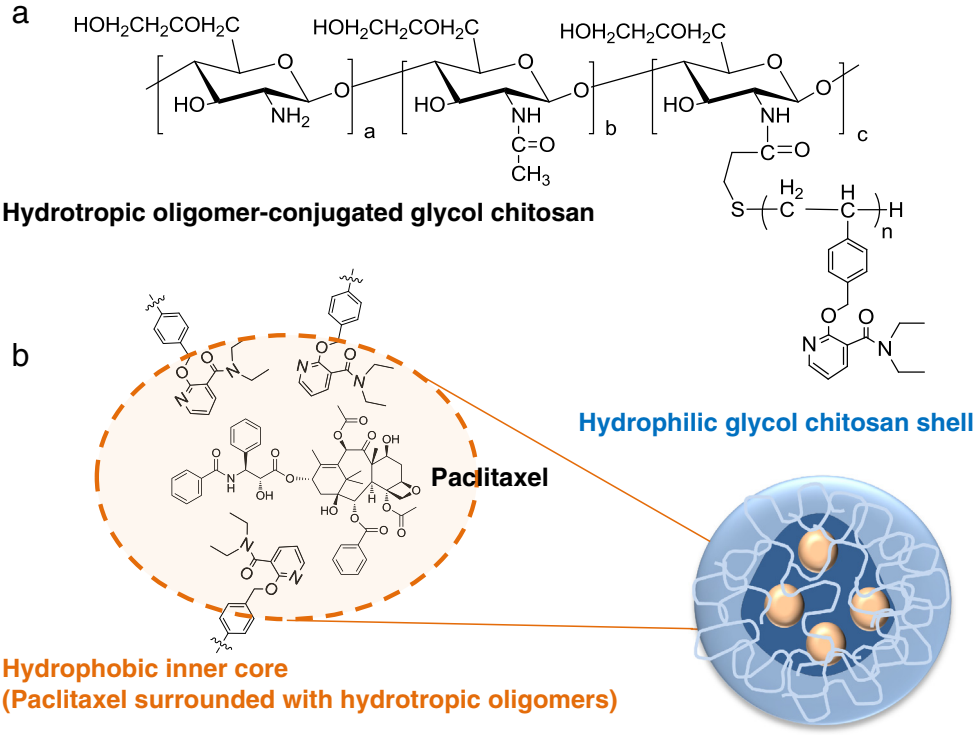

Scheme 1. Hydrotropic oligomer-conjugated glycol chitosan nanoparticles (HO-CNPs). (a) Chemical structure of HO-CNPs. (b) Amphiphilic self-assembly of PTX-encapsulated HO-CNPs (PTX-HO-CNPs).

reaction was initiated by 4.43 and 3.86 mg of EDAC and HOBt, respectively (1.5 M eq. of oligo(VBODENA)-COOH). The resulting solution was stirred for 1 day at room temperature. Then, the solution was dialyzed for 1 day using a membrane tube (MW cutoff = 12,000–14,000) against water and methanol. The resulting conjugate was freeze-dried and freshly solubilized at every experiment. For fluorescence imaging, five molecules of hydroxysuccinimide-activated Cy5.5 were conjugated to one HO-CNP. Unconjugated Cy5.5 was removed by dialysis for 1 day using a membrane tube (MW cutoff = 12,000–14,000) against water and methanol.

2.3. Preparation of paclitaxel-encapsulated HO-CNPs (PTX-HO-CNPs)

Paclitaxel was encapsulated into HO-CNPs by a simple dialysis method [19]. HO-CNPs (100 mg) were dissolved in 4 ml of distilled water/methanol (50:50, v/v) solution. Then, different amount of PTXs (10–30 mg) in 2 ml of methanol was added to this solution. The resulting solution was dialyzed for 2 days against distilled water using a dialysis tube (MW cutoff = 12,000–14,000) to remove the unloaded PTX. Then, it was centrifuged at 10,000 ×*g* for 30 min to completely remove free PTX, and the upper solution was lyophilized to obtain PTX-encapsulated HO-CNPs (PTX-HO-CNPs). PTX-loading amount and efficiency within nanoparticles was measured using the high performance liquid chromatography (HPLC, Aglient Technologies, Wilmington, DE). The mobile phase, consisting of acetonitrile/water (45:55, v/v) co-solvent, was delivered at a flow rate of 1.0 ml/min. Eluted compounds were detected at 227 nm using a Spectra 100 UV–Vis detector.

The particle sizes of nanoparticles were measured by using dynamic light scattering (DLS) (127-35 laser, Spectra Physics, Mountain View, CA) at 1 mg/ml in PBS. The zeta-potential value was measured by 90 Plus particle size analyzer (Brookhaven Instruments Corporation). The morphological shapes of nanoparticles were analyzed using transmission electron microscopy (TEM) (CM30 electron microscope, Philips, CA), operated at an acceleration voltage of 80 kV. Each sample (1 mg/ml in distilled water) was placed on a 300-mesh copper grid coated with carbon. After drying the sample, negative staining was performed using a droplet of 2 wt.% uranyl acetate.

2.4. Paclitaxel release from PTX-HO-CNPs

We determined the PTX release from PTX-HO-CNPs (10, 20, and 30 wt.% PTX feed) using 0.1 M sodium salicylate solution to make a sink condition as reported previously [20]. The lyophilized nanoparticles (1 mg) were dispersed in 1 ml of PBS (pH 7.4) and moved to a cellulose ester membrane tube (molecular weight cutoff = 8000, Spectrum®). Then, they were sunk in 30 ml of PBS (pH 7.4) and gently shaken at 80 rpm in water bath at 37 °C. At given times, the medium was replaced with fresh medium. The amount of PTX was measured using the high performance liquid chromatography (HPLC).

2.5. Cellular uptake and cytotoxicity of PTX-HO-CNPs

MDA-MB231 human breast cancer cells were purchased from the American Type Culture Collection (Rockville, MD). They were cultured in RPMI 1640 (Gibco, Grand Island, NY) containing 10% (v/v) FBS (Gibco) and 1% (w/v) penicillin–streptomycin at 37 °C in a humidified incubator with 5% CO_2. To test the cellular uptake of PTX-HO-CNPs, cells were seeded onto 35 mm coverglass bottom dishes and incubated up to the cell confluence of 60–80%. After washing the cells twice with PBS, the cells were incubated in a serum-free medium containing Cy5.5 labeled PTX-HO-CNPs (10 μg/ml of PTX) for 2 h. For the cellular images, PTX-HO-CNPs-treated cells were washed twice with PBS, followed by fixation with 4% paraformaldehyde for 5 min. Finally, the cells were mounted with Fluoromount-G™ (SouthernBiotech, Birmingham, AL) and the cell images were observed using a FluoView FV1000 confocal laser scanning microscope (Olympus, Tokyo, Japan) equipped with HeNe-Red (633 nm) laser.

The cytotoxicity of PTX formulation containing 50/50% Cremophor EL/ethanol mixture, Cremophor EL, HO-CNPs, and PTX-HO-CNPs were evaluated using 3-(4,5-dimethylthiazol-2-yl)-2,5-diphenyltetrazolium bromide (MTT) assay. Cells were seeded at a density of 1×10^4 cells/well in 96-well plates, and incubated overnight. PTX solution was prepared at 6 mg/ml by mixing 200 μl of PTX in ethanol (12 mg/ml) with same volume of Cremophor EL and sonicated for 30 min. The cells were washed twice with PBS and incubated with various concentrations of each sample. For convenience, the amounts of bare HO-CNP or Cremophor EL without PTX in graph were described as the concentrations of PTX which were used in equivalent amounts of PTX-HO-CNPs or PTX formulation. After incubation for 2 days, they washed twice with PBS and culture medium was replaced with fresh RPMI 1640 without FBS. Then, 10 μl of MTT solution (5 mg/ml in PBS) was added to each well. After further incubation for 4 h, the media were removed and the cells were dissolved in DMSO. Absorbance was measured at 570 nm with a microplate reader (VERSAmax™, Molecular Devices Corp., Sunnyvale, CA).

After treatment of samples, HO-CNP, and PTX-HO-CNPs, apoptotic cells were monitored using fluorescence microscopy, as follows. MDA-MB231 cells were seeded onto 35 mm gelatin-coated coverslips in 12-well plates (3×10^4 cells per well) and allowed to grow until a confluence of 80%. The cells were washed twice with PBS and incubated with PTX formulation, HO-CNPs, and PTX-HO-CNPs (50 μg/ml PTX) for 1 day. For assessing apoptotic cells by FITC labeled annexin (annexin-V-FITC), cells were washed twice with PBS and incubated with annexin-V-FITC fluorescence microscopy kit (0.5 μg/ml, BD Bioscience, San Jose, CA) for 15 min in the dark condition. Following washing with binding buffer, cells were observed under the IX81-ZDC focus drift compensating microscope (Olympus, Tokyo, Japan).

2.6. In vivo and ex vivo NIRF imaging of Cy5.5 labeled PTX-HO-CNPs

All experiments with animals were performed in compliance with the relevant laws and institutional guidelines of Korea Institute of Science and Technology (KIST) and institutional committees have approved the experiments. Athymic nude mice (20 g, Institute of Medical Science, Tokyo) were used for *in vivo* experiments. Subcutaneous tumor models were established by inoculating 1×10^7 MDA-MB231 human breast cancer cells into the dorsal side of mice. When tumors grew to approximately 200–250 mm^3 in volume, Cy5.5-labeled PTX-HO-CNPs (20 wt.% PTX, 5 mg/kg of PTX in 100 μl of saline) and Cy5.5-labeled Abraxane® (10 wt.% PTX, 5 mg/kg of PTX in 100 μl of saline) were injected *via* the tail vein into MDA-MB-231 tumor-bearing mice. After injection of samples, the time-dependent accumulation of nanoparticles in tumor site were non-invasively imaged using the eXplore Optix System (Advanced Research Technologies Inc., Montreal, Canada) [21]. For the imaging study, laser power, exposure time and count time setting were optimized at 30 μW and 0.3 s per point. Near-infrared fluorescence (NIRF) emission (600–700 nm) was detected with a fast photomultiplier tube (Hamamatsu, Japan) and a time-correlated single photon counting system (Becker and Hickl GmbH, Berlin, Germany). All data are calculated using the region-of-interest (ROI) function of Analysis Workstation software (ART Advanced Research Technologies Inc., Montreal, Canada) and data are given as mean ± S.D. for a group of three animals. To analyze the organ distribution of each nanoparticle, the mice were sacrificed 3 days post-injection of the samples, and major organs (livers, lungs, spleens, kidneys, and hearts) and tumors were excised. The NIRF signal intensity in tissues was measured and imaged using a 12-bit CCD camera (Imaging Station 4000 MM; Kodak, New Haven, CT) equipped with a Cy5.5 emission filter sets (600 to 700 nm; Omega Optical) [22]. A quantification of NIRF signals was performed as total photons per centimeter squared per steradian ($p/s/cm^2/sr$) per each tumor ($n = 5$ mice per group).

2.7. Intravital imaging of PTX-HO-CNPs

Intravital real-time images of tumor tissues were obtained using an Olympus IV100 Intravital Scanning Laser Microscope (Olympus Corp., Tokyo, Japan) [23]. To visualize tumor tissue, red fluorescence protein (RFP)-labeled B16F10 cells (1×10^6 cells/mouse) were subcutaneously implanted in the dorsa of a nude mouse and allowed to grow for 12 days. When tumors grew to approximately 200–250 mm^3 in volume, the mice was anesthetized (2% isoflurane in 2 l/min O_2). Then, the tumor tissue was exposed by making an incision in the skin at the tumor site, followed by intravenous injection of fluorescein isothiocyanate (FITC)-labeled dextran (10 mg/kg) to visualize the tumor vasculature. The real-time imaging of Cy5.5-labeled PTX-HO-CNPs (20 wt.% PTX, 5 mg/kg of PTX in 100 μl of saline) was monitored in the tumor tissue for 6 h.

2.8. In vivo therapeutic efficacy of PTX-HO-CNPs in tumor-bearing mice

The subcutaneous dorsa of athymic nude female mice (6 weeks old; 20 g) were inoculated with 1×10^7 MDA-MB231 human breast cancer cells. Mice were divided into four groups ($n = 7$), and treated with one of the following materials: (i) saline, (ii) PTX formulation (20 mg/kg), (iii) Abraxane® (20 mg/kg PTX), and (iv) PTX-HO-CNPs (20 mg/kg PTX). When tumor volume became 100–150 mm^3 in volume, each treatment was administered *via* a tail vein every three days for 15 days. The tumor volumes of each tumor-bearing mouse were recorded for 34 days. The length and width of the tumors were measured by digital calipers, calculating tumor volume using the following formula: $(\text{width}^2 \times \text{length})/2$. Also, the survival rate of each group was recorded for 34 days.

Apoptotic cells in tumor tissues were histologically evaluated with DAPI staining and terminal deoxynucleotidyl transferasemediated nick end labeling (TUNEL) assays, with commercial apoptosis detection kit (Promega Corp., WI) [24]. The apoptotic cells in tissues were also determined by TUNEL assay and the slides were counterstained with DAPI. TUNEL data were analyzed by a researcher blind to the nature, at ×400 magnification, using a computer-aided light microscope.

2.9. Statistics

The statistical significance of differences between experimental and control groups was determined using a Student's *t*-test. P values < 0.05 were considered significant, and significant differences are shown by asterisks in the Figures.

3. Results and discussion

3.1. Preparation and characterization of PTX-HO-CNPs

In this study, we developed the glycol chitosan nanoparticles with hydrotropic oligomers (HO-CNPs) as a new tumor-targeting drug delivery system. For enhancing drug-loading amount of PTX in drug carriers, hydrotropic oligomers, oligo(2-(4-(vinylbenzyloxy)-N, N-diethylnicotinamide) (oligo(VBODENA-COOH)), were directly conjugated to glycol chitosan polymers (Scheme 1a). The calculated ratio of a: b:c is about 79.5:17.3:3.2. The DENA moiety showed the high solubilizing ability for PTX among various hydrotropic agents [20]. Also, this hydroptic oligomer would be useful for the hydrophobic moiety in the glycol chitosan nanoparticles that may allow formation of self-assembled nanoparticles that can encapsulate large amounts of PTX (Scheme 1b).

The HOs, oligo(VBODENA)-COOH, were synthesized by free radical chain transfer polymerization of VBODENA monomer using MPA as a chain transfer agent. The produced HOs had a narrow number-average molecular weight of 3.52 kDa, confirmed by ^{1}H NMR spectrum (VBODENA at 0.89 ppm and 1.04 ppm, MPA at 2.82 ppm). Then, they were conjugated to hydrophilic glycol chitosan polymers by amide

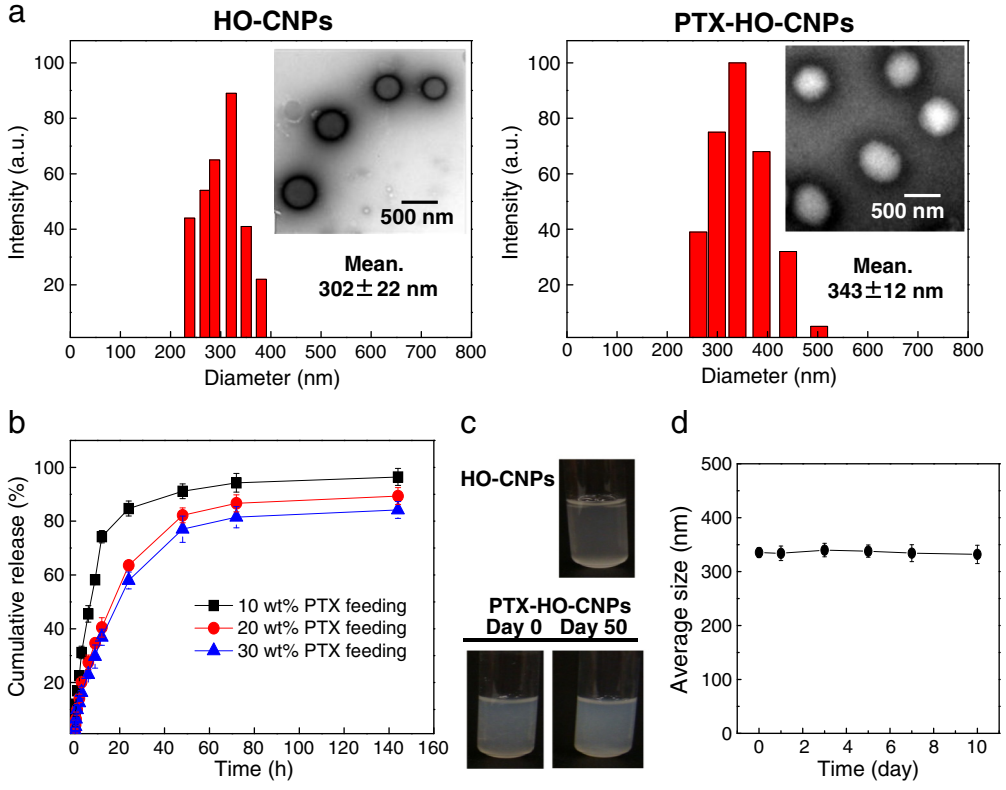

Fig. 1. Characterization and drug release profile of PTX-HO-CNPs. (a) Size and shape of HO-CNPs and PTX-HO-CNPs. (b) Time-dependent PTX release from PTX-HO-CNPs. (c) Stability of PTX-HO-CNPs in PBS for 50 days. (d) Particle size of PTX-HO-CNP (1 mg/ml) at 37 °C in PBS as a function of time.

Table 1
Characteristics of HO-CNP and PTX-HO-CNP.

Sample	Feed ratio of PTX (wt.%)	Loading amout of PTX[a] (wt.%)	Loading efficiency[b] (%)	Size[c] (nm)
HO-CNP	–	–	–	302 ± 22
PTX (10 wt.%)-HO-CNP	10	9.6 ± 0.2	96.8 ± 2.5	328 ± 18
PTX (20 wt.%)-HO-CNP	20	19.2 ± 0.6	95.1 ± 3.3	343 ± 12
PTX (30 wt.%)-HO-CNP	30	24.2 ± 0.3	78.4 ± 0.9	358 ± 21

[a] Loading amount of PTX in nanoparticles were measured using HPLC.
[b] Loading efficiency of PTX in nanoparticles were calculated from the ratio of loading content of PTX/feed amount of PTX in the nanoparticles.
[c] Average size of each nanoparticle (1 mg/ml in PBS at 37 °C) was measured using dynamic light scattering.

bond linkages. Based on ^{1}H NMR data, we estimated that about 40 of oligo(VBODENA-COOH; 1.00 ppm and 1.20 ppm) were conjugated to one glycol chitosan backbone. The resulting amphiphilic hydrotropic oligomer-glycol chitosan conjugates (HO-GCs) self-assembled into the nanoparticle structure in aqueous condition. They were 302 ± 22 nm in size with narrow size distribution in dynamic light scattering (DLS) data and spherical shapes in transmission electron microscopy (TEM) images (Fig. 1a). In this structure, hydrophilic glycol chitosan shell can prevent the aggregation of nanoparticles with each other or with serum proteins, whereas the inner cores of hydrophobic HOs can solubilize the water-insoluble PTX into the HO-CNPs with high drug-loading efficiency.

The water-insoluble drug, PTX, was readily encapsulated in the HO-CNPs by simple dialysis methods, in resulting PTX-encapsulated HO-CNPs (PTX-HO-CNPs) [19]. The drug-loading efficiencies were about 96.8, 95.1, and 78.4%, when the feed ratio of PTX against HO-CNPs were about 10, 20, and 30 wt.%, respectively (Table 1). They showed over 95% loading efficiency at 20 wt.% PTX feed ratio which is much higher than the cases of other nanoparticles. Generally, it was reported that the drug-loading amount of PTX was about 10 wt.% in the nanoparticles [25]. With PTX feed ratio higher than 30 wt.%, the loading efficiencies dropped to less than 50% showing large loss of drugs. Consequently, we used 20 wt.% PTX feed ratio during the following *in vitro* and *in vivo* experiments, wherein the PTX amount in the nanoparticles was about 19.2 wt.%. After loading of PTX, the size of PTX-HO-CNPs slightly increased to about 343 ± 12 nm while maintaining their spherical shapes. The zeta-potential value of PTX-HO-CNPs was 13.09 ± 0.42 mV in PBS (pH 7.4). The time-dependent release of PTX from PTX-HO-CNPs was determined in the sink condition with sodium salicylate. All nanoparticles showed sustained release of PTX during about three days (Fig. 1b). Interestingly, the release rate was even slower in the case of 20 and 30 wt.% PTX feed ratio, compared to the case of

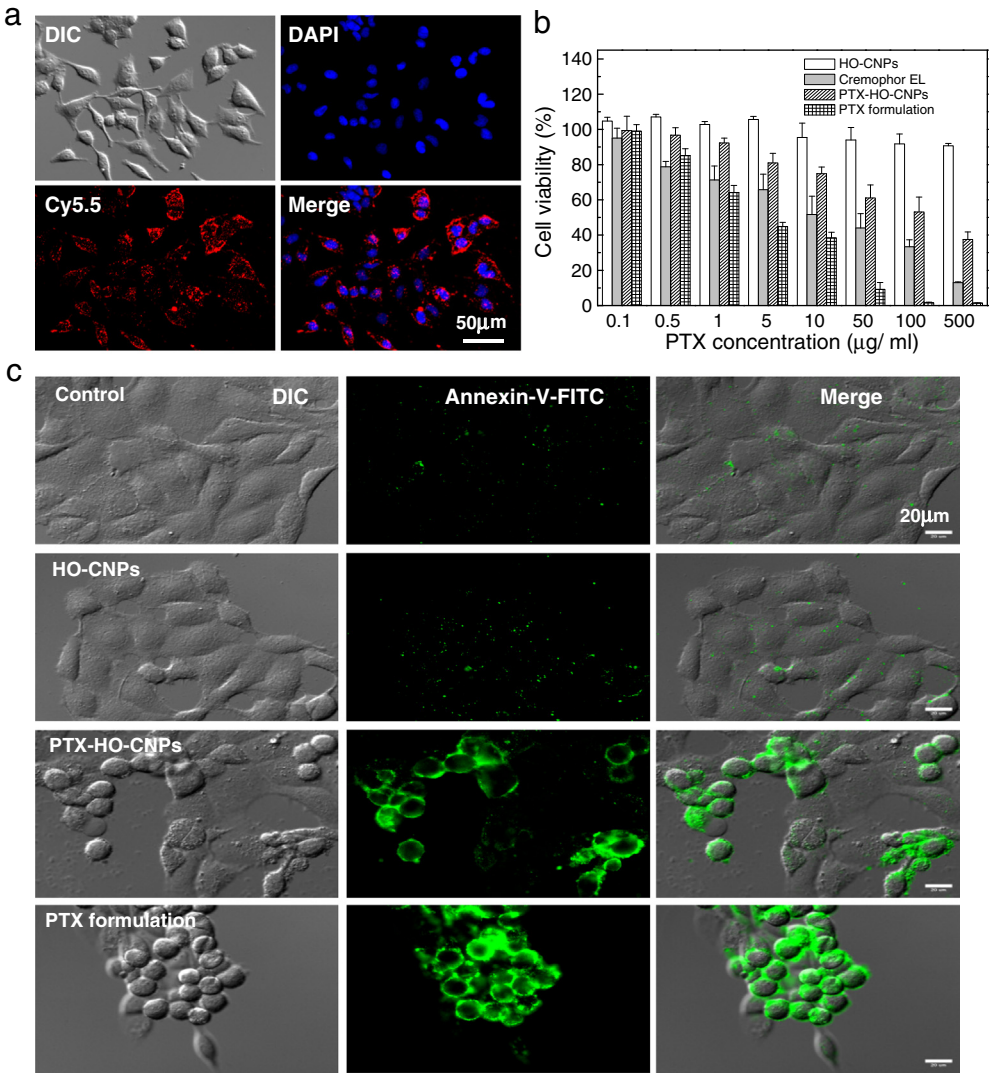

Fig. 2. (a) Cellular uptake of Cy5.5-labeded PTX-HO-CNPs in MDA-MB-231 tumor cells. (b) Cell viability test with HO-CNPs and PTX-HO-CNPs in MDA-MB-231 tumor cells. (c) Apoptosis imaging of PTX-HO-CNPs-treated MDA-MB-231 tumor cells using annexin V-FITC.

10 wt.% PTX feed ratio. This result demonstrates that PTX-HO-CNPs are in very stable conditions surrounded by hydrotropic oligomers even in the case of high feed ratio. Theoretically, one PTX molecule is surrounded by 5.36 hydrotropic oligomers inside the nanoparticles with 20 wt.% PTX feed ratio. In this condition, they showed no aggregation at 1 mg/ml nanoparticle in PBS (pH 7.4) for 50 days (Fig. 1c and d). Their size did not change for more than 50 days in our previous paper [16]. It showed that about 1.17 mM of VBODENA oligomers within nanoparticles could solubilize 0.196 mg/ml of PTX, which is more effective in solubilizing PTX than the case of free DENA molecules [15]. This result may be due to the physical loading of PTX into small nanoparticles which helps the hydrotropic interaction between PTX and DENA molecules.

3.2. In vitro cellular uptake and cytotoxicity of PTX-HO-CNPs

In order to deliver PTX into tumor cells, PTX-HO-CNPs should be internalized into cells and release the encapsulated PTX inside cells. Thus, we observed the cellular uptake of Cy5.5-labeled PTX-HO-CNPs in the cell culture system (Fig. 2a). After incubation of PTX-HO-CNPs (10 μg/ml of PTX) in MDA-MB231 human breast cancer cells for 2 h, many nanoparticles were clearly observed inside cells and evenly dispersed in the cytosol as seen in time-lapse imaging. We already reported that glycol chitosan nanoparticles exhibited a fast cellular uptake through clathrin-mediated endocytosis, caveolae, and macropinocytosis [26]. This rapid cellular uptake of PTX-HO-CNPs in cell culture system may serve as a potential drug carrier for the intracellular delivery of PTX in cancer treatment.

In vitro cell viability of PTX-HO-CNPs was evaluated by MTT assay and microscopic imaging with annexin V-FITC. In the MTT assay, HO-CNPs without PTX showed negligible cytotoxicity on MDA-MB-231 human breast cancer cells. More than 90% of cells were alive even after treatment of about 2.5 mg/ml of HO-CNPs which can encapsulate 500 μg/ml PTX (Fig. 2b). This result is a good comparison to the case of Cremophor EL which showed severe cytotoxicity at high concentrations. It showed the biocompatibility of HO-CNPs as drug carriers, and it is expected to result in fewer side effects than Cremophor EL. On the contrary, PTX-HO-CNPs significantly inhibit the proliferation and division of MDA-MB-231 tumor cells, showing that the therapeutic ability

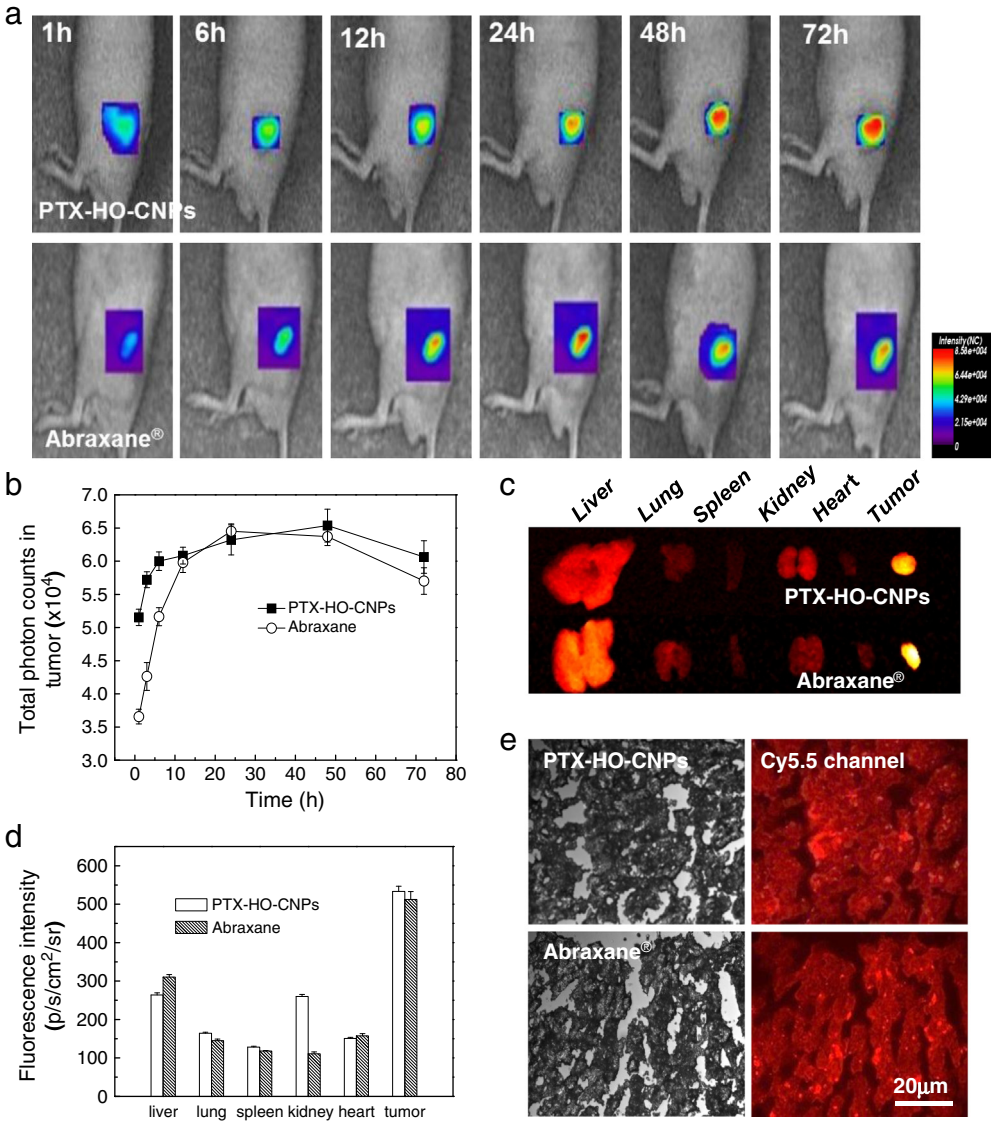

Fig. 3. *In vivo* imaging of tumor-bearing mice injected with PTX-HO-CNPs. (a) NIRF images of tumor site after intravenous injection of Cy5.5-labeled PTX-HO-CNPs and Cy5.5-labeled Abraxane®. (b) NIRF signal intensity in tumor site of Cy5.5-labeled PTX-HO-CNPs and Cy5.5-labeled Abraxane®-treated mice. (c) *Ex vivo* organ and tumor images of PTX-HO-CNPs and Abraxane®-treated mice after 72 h post-injection. (d) NIRF signal intensity of excised organs and tumors after 72 h post-injection of PTX-HO-CNPs and Abraxane® (e) NIRF images of sliced tumor tissue of PTX-HO-CNPs and Abraxane®-treated mice after 72 h post-injection (n = 3).

of PTX is still active. As expected, large amounts of apoptotic cells were observed in PTX-HO-CNPs-treated cells after treatment of annexin V-FITC. The treatment of bare HO-CNPs did not show a significant change of cells. However, intense green fluorescence was observed after treatment of PTX-HO-CNPs which was similar with the case of PTX formulation containing a 50/50% Cremophor EL/ethanol mixture (Fig. 2c). These results showed the possibility of PTX-HO-CNP as biocompatible and effective carrier for PTX delivery.

3.3. In vivo biodistribution of PTX-HO-CNPs in tumor bearing mice

Encouraged by these *in vitro* results, we moved to *in vivo* experiments with tumor-bearing mice. We compared the tumor-targeting and therapeutic ability of PTX-HO-CNPs with Abraxane® during *in vivo* experiments. Abraxane® is the most representative nanoparticle formulation of PTX, which are commercialized and generally used in clinic now [17]. To track the location of PTX-HO-CNPs and Abraxane®, both nanoparticles were labeled with Cy5.5, near-infrared fluorescence (NIRF) dye. Then, the biodistribution of each nanoparticle was analyzed by *in vivo* and *ex vivo* optical imaging after their intravenous injection to MDA-MB-231 tumor-bearing mice.

In time-dependent NIRF images, the tumor tissues on the dorsal side could be easily delineated from surrounding normal tissues by intense fluorescence in mice treated with Cy5.5 labeled PTX-HO-CNPs (20 wt.% PTX, 5 mg/kg of PTX in 100 μl of saline) and Cy5.5-labeled Abraxane® (10 wt.% PTX, 5 mg/kg of PTX in 100 μl of saline) (Fig. 3a). Both nanoparticles showed high accumulation in tumor tissue and the fluorescence intensity in tumor tissues maximized 48 h post-injection (Fig. 3b). This result may be originated from EPR effect of nanoparticles through fenestrated vessels in angiogenic tumor tissue. The amount of PTX in PTX-HO-CNPs was about two fold larger than that of Abraxane®. Consequently, this result demonstrates that PTX-HO-CNPs can show high tumor accumulation similar with Abraxane® while it contaINS two-fold PTX. In accordance with these *in vivo* images, the tumor tissues showed intense fluorescence under the *ex vivo* condition 3 days post-injection of nanoparticles (Fig. 3c). Interestingly, PTX-HO-CNPs showed high fluorescence in the kidney next to the tumor, while the liver is brighter in the case of Abraxane®-treated mice (Fig. 3d). This result showed that PTX-HO-CNPs is mainly excreted from the body by renal clearance of the kidney, but Abraxane® used reticuloendothelial (RES) system of the liver. Sliced tumor tissue images also showed widespread NIRF spots meaning abundant nanoparticles in cases of both PTX-HO-CNPs and Abraxane® (Fig. 3e).

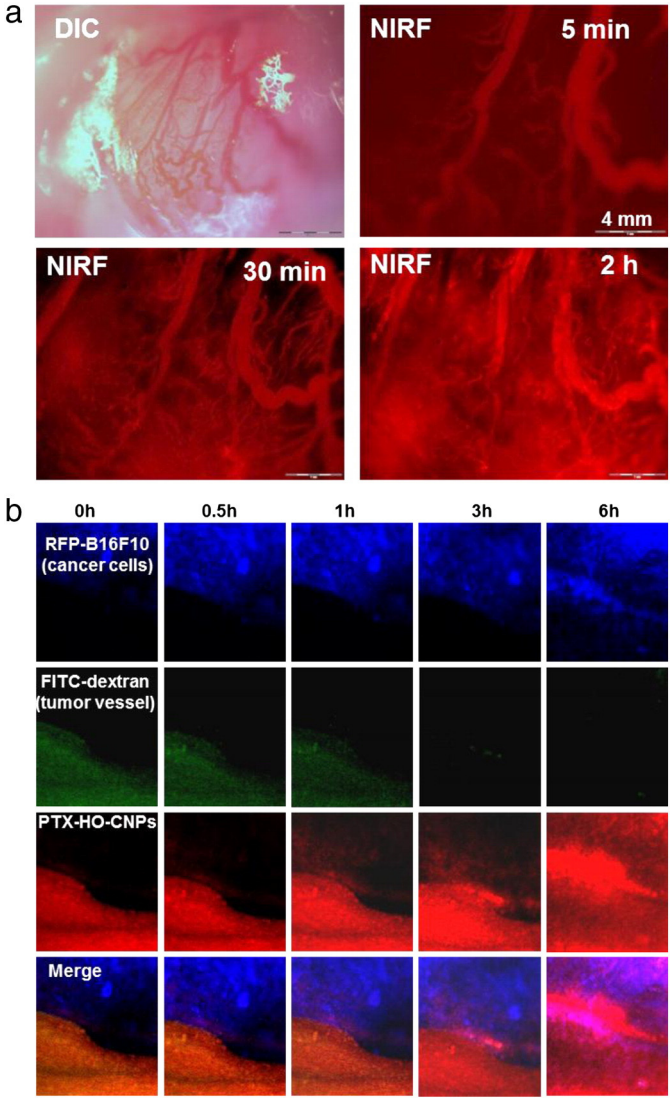

Fig. 4. Intravital imaging of tumor-bearing mice injected with Cy5.5-labeled PTX-HO-CNPs; (a) single NIRF channel image and (b) multiple fluorescence channel image.

3.4. Intravital imaging of PTX-HO-CNPs in tumor bearing mice

For precise imaging of nanoparticles, we performed intravital imaging in the tumor tissue of mice. Intravital imaging can directly access the target tissue under *in vivo* condition and provide higher resolution microscopic images than the case of whole body imaging [27]. With the Olympus IV100 intravital imaging machine, we could observe time-dependent movement of Cy5.5-labeled PTX-HO-CNPs after an intravenous injection to tumor-bearing mice [23]. As time passed, they could pass through fenestrate tumor vessels and move to the surrounding tumor cells (Fig. 4a). Then, this extravasation of PTX-HO-CNPs was shown in three color fluorescence images with even higher resolutions. We used tumor-bearing mice which were prepared with B16F10 tumor cells stably expressing red fluorescence protein (RFP). To observe the area of tumor vessels, we intravenously injected FITC-labeled dextran simultaneously with Cy5.5-labeled PTX-HO-CNPs.

In the initial time, FITC-dextran (green) and fluorescence of FITC-dextran disappeared due to short circulation time. However, PTX-HO-CNPs gradually moved from tumor vessels to surrounding tumor cells and large amount of them accumulated in tumor cells 6 h post-injection. These images showed EPR effect of PTX-HO-CNPs in living tumor tissue, which is a potential advantage of PTX-HO-CNPs for tumor-targeting delivery system.

3.5. Therapeutic efficacy of PTX-HO-CNPs in tumor bearing mice

Finally, we evaluated the therapeutic efficacy of PTX-HO-CNPs in the same MDA-MB-231 tumor-bearing mice and compared it with the cases of PTX formulation containing 50/50% Cremophor EL/ethanol mixture and Abraxane®, wherein the PTX concentration in each sample is mostly matched to 20 mg/kg. Thirty-four days post-injection, the tumor volume of mice treated with saline grew to about 2700 mm^3 (Fig. 5a). In the case of PTX formulation, it reached to about 1300 mm^3 showing insufficient suppression of tumor growth. The mice treated with Abraxane® and PTX-HO-CNPs showed smaller tumor size, and there was only negligible tumor growth especially in the case of PTX-HO-CNPs. After treatment and observation, there were two dead mice in the groups treated with saline and PTX formulation, respectively (Fig. 5b). However, all mice were still alive in the cases of Abraxane® and PTX-HO-CNPs showing the higher therapeutic efficacy and safety, compared to PTX formulation in cancer treatment. After therapy, the mice were sacrificed and the tumor tissues of each group were obtained and compared with each other. As expected, tumor tissues of PTX-HO-CNPs-treated mice were smaller than that of other tumor tissues (Fig. 5c). The average weight was about 10.7, 6.3, and 2.8 fold smaller

than the case of saline, PTX formulation, and Abraxane®, respectively (Fig. 5d). Then, these tumor tissues were further analyzed by histological staining. After TUNEL assay, the amount of red fluorescent spots was much larger in the tumor tissue of mice treated with PTX-HO-CNPs, compared to all other groups (Fig. 5e). These images showed that there was a large amount of cell death in PTX-HO-CNPs-treated tumor tissue and that maybe originated that effectively delivered PTX in targeted tumor tissues.

4. Conclusion

For efficient drug-loading and tumor-targeting therapy, we developed hydrotropic oligomer-conjugated glycol chitosan nanoparticles. This nanoparticle maintained stable nanoparticle structure in PBS for more than 50 days while containing a high amount of PTX up to 20 wt.% in the nanoparticles. The hydrotropic oligomer-conjugated glycol chitosan nanoparticles are non-toxic, and they showed significant anticancer effect after PTX encapsulation. When injected intravenously to mice, these nanoparticles showed superior tumor-targeting ability. The time-dependent intravital images enabled precise observation of their penetration through tumor vessels and accumulation in tumor tissue. Furthermore, the data of *in vivo* tumor therapy showed that their therapeutic efficacy outperformed Abraxane®, commercialized nano-formulation of PTX even with much lower amount of carrier used. These overall results demonstrate that our nanoparticle is a promising tumor-targeting nano-carrier for PTX delivery.

Acknowledgments

This work is supported by the GRL Program, the M.D.-Ph.D. Program (2010-0019863, 2010-0019864), and the Fusion Technology Project (2009-0081876) of MEST and Intramural Research Programs (Young Fellow) of KIST.

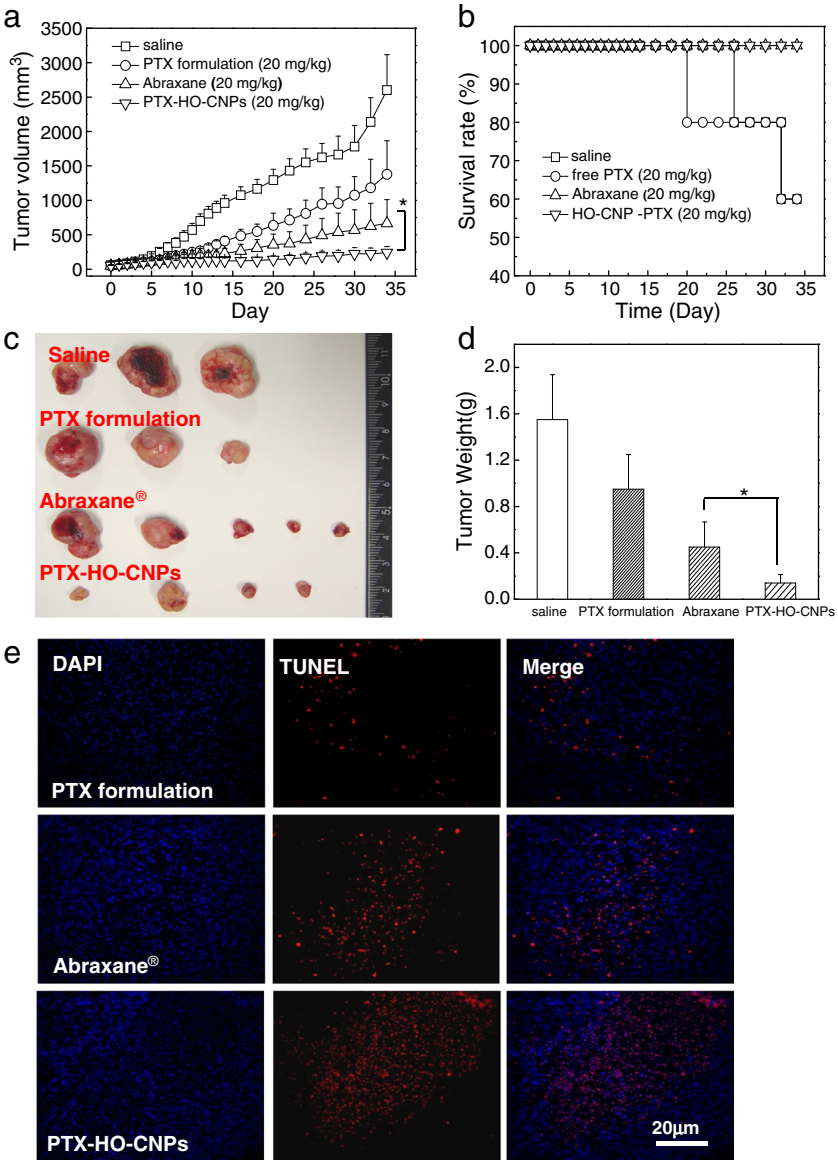

Fig. 5. *In vivo* tumor therapy of tumor-bearing mice with PTX-HO-CNPs. (a) Time-dependent tumor growth profile of tumor-bearing mice injected with saline, PTX formulation, Abraxane®, and PTX-HO-CNPs (n = 7). (b) Survival rate of PTX-HO-CNPs-treated mice. (c) Excised tumor images after tumor therapy. (d) Tumor weights after post-injection of PTX-HO-CNPs. (e) Histological analysis of tumor tissue after tumor therapy with PTX-HO-CNPs (blue: DAPI for nucleus staining, red: TUNEL for the imaging of cell death). (For interpretation of the references to color in this figure , the reader is referred to the web version of this article.)

References

[1] Z. Cheng, A. Al Zaki, J.Z. Hui, V.R. Muzykantov, A. Tsourkas, Multifunctional nanoparticles: cost versus benefit of adding targeting and imaging capabilities, Science 338 (2012) 903–910.

[2] R.A. Petros, J.M. DeSimone, Strategies in the design of nanoparticles for therapeutic applications, Nat. Rev. Drug Discov. 9 (2010) 615–627.

[3] H. Koo, M.S. Huh, J.H. Ryu, D.-E. Lee, I.-C. Sun, K. Choi, K. Kim, I.C. Kwon, Nanoprobes for biomedical imaging in living systems, Nano Today 6 (2011) 204–220.

[4] V.P. Torchilin, Recent advances with liposomes as pharmaceutical carriers, Nat. Rev. Drug Discov. 4 (2005) 145–160.

[5] Y. Matsumura, Preclinical and clinical studies of NK012, an SN-38-incorporating polymeric micelles, which is designed based on EPR effect, Adv. Drug Deliv. Rev. 63 (2011) 184–192.

[6] H. Koo, M.S. Huh, I.-C. Sun, S.H. Yuk, K. Choi, K. Kim, I.C. Kwon, *In vivo* targeted delivery of nanoparticles for theranosis, Acc. Chem. Res. 44 (2011) 1018–1028.

[7] V. Torchilin, Tumor delivery of macromolecular drugs based on the EPR effect, Adv. Drug Deliv. Rev. 63 (2011) 131–135.

[8] J.D. Byrne, T. Betancourt, L. Brannon-Peppas, Active targeting schemes for nanoparticle systems in cancer therapeutics, Adv. Drug Deliv. Rev. 60 (2008) 1615–1626.

[9] K.H. Min, K. Park, Y.-S. Kim, S.M. Bae, S. Lee, H.G. Jo, R.-W. Park, I.-S. Kim, S.Y. Jeong, K. Kim, I.C. Kwon, Hydrophobically modified glycol chitosan nanoparticles-encapsulated camptothecin enhance the drug stability and tumor targeting in cancer therapy, J. Control. Release 127 (2008) 208–218.

[10] H.Y. Yoon, H. Koo, K.Y. Choi, I. Chan Kwon, K. Choi, J.H. Park, K. Kim, Photo-crosslinked hyaluronic acid nanoparticles with improved stability for *in vivo* tumor-targeted drug delivery, Biomaterials 34 (2013) 5273–5280.

[11] C. Som, B. Nowack, H.F. Krug, P. Wick, Toward the development of decision supporting tools that can be used for safe production and use of nanomaterials, Acc. Chem. Res. 46 (2012) 863–872.

[12] M.V. Blagosklonny, T. Fojo, Molecular effects of paclitaxel: myths and reality (a critical review), Int. J. Cancer 83 (1999) 151–156.

[13] H. Gelderblom, J. Verweij, K. Nooter, A. Sparreboom, Cremophor EL: the drawbacks and advantages of vehicle selection for drug formulation, Eur. J. Cancer 37 (2001) 1590–1598.

[14] D. Loven, H. Levavi, G. Sabach, R. Zart, M. Andras, A. Fishman, Y. Karmon, T. Levi, R. Dabby, N. Gadoth, Long-term glutamate supplementation failed to protect against peripheral neurotoxicity of paclitaxel, Eur. J. Cancer Care 18 (2009) 78–83.

[15] J. Lee, S. Lee, G. Acharya, C.-j. Chang, K. Park, Hydrotropic solubilization of paclitaxel: analysis of chemical structures for hydrotropic property, Pharm. Res. 20 (2003) 1022–1030.

[16] G. Saravanakumar, K.H. Min, D.S. Min, A.Y. Kim, C.-M. Lee, Y.W. Cho, S.C. Lee, K. Kim, S.Y. Jeong, K. Park, J.H. Park, I.C. Kwon, Hydrotropic oligomer-conjugated glycol chitosan as a carrier of paclitaxel: synthesis, characterization, and *in vivo* biodistribution, J. Control. Release 140 (2009) 210–217.

[17] F. Kratz, Albumin as a drug carrier: design of prodrugs, drug conjugates and nanoparticles, J. Control. Release 132 (2008) 171–183.

[18] S.C. Lee, K.M. Huh, J. Lee, Y.W. Cho, R.E. Galinsky, K. Park, Hydrotropic polymeric micelles for enhanced paclitaxel solubility: *in vitro* and *in vivo* characterization, Biomacromolecules 8 (2006) 202–208.

[19] H.Y. Yoon, H. Koo, K.Y. Choi, S.J. Lee, K. Kim, I.C. Kwon, J.F. Leary, K. Park, S.H. Yuk, J.H. Park, K. Choi, Tumor-targeting hyaluronic acid nanoparticles for photodynamic imaging and therapy, Biomaterials 33 (2012) 3980–3989.

[20] K.M. Huh, S.C. Lee, Y.W. Cho, J. Lee, J.H. Jeong, K. Park, Hydrotropic polymer micelle system for delivery of paclitaxel, J. Control. Release 101 (2005) 59–68.

[21] H. Koo, S. Lee, J.H. Na, S.H. Kim, S.K. Hahn, K. Choi, I.C. Kwon, S.Y. Jeong, K. Kim, Bioorthogonal copper-free click chemistry *in vivo* for tumor-targeted delivery of nanoparticles, Angew. Chem. Int. Ed. 51 (2012) 11836–11840.

[22] H. Koo, H. Lee, S. Lee, K.H. Min, M.S. Kim, D.S. Lee, Y. Choi, I.C. Kwon, K. Kim, S.Y. Jeong, *In vivo* tumor diagnosis and photodynamic therapy via tumoral pH-responsive polymeric micelles, Chem. Commun. 46 (2010) 5668–5670.

[23] K.Y. Choi, K.H. Min, H.Y. Yoon, K. Kim, J.H. Park, I.C. Kwon, K. Choi, S.Y. Jeong, PEGylation of hyaluronic acid nanoparticles improves tumor targetability *in vivo*, Biomaterials 32 (2011) 1880–1889.

[24] K.H. Min, J.-H. Kim, S.M. Bae, H. Shin, M.S. Kim, S. Park, H. Lee, R.-W. Park, I.-S. Kim, K. Kim, I.C. Kwon, S.Y. Jeong, D.S. Lee, Tumoral acidic pH-responsive MPEG-poly ([beta]-amino ester) polymeric micelles for cancer targeting therapy, J. Control. Release 144 (2010) 259–266.

[25] J.H. Kim, Y.S. Kim, S. Kim, J.H. Park, K. Kim, K. Choi, H. Chung, S.Y. Jeong, R.W. Park, I.S. Kim, I.C. Kwon, Hydrophobically modified glycol chitosan nanoparticles as carriers for paclitaxel, J. Control. Release 111 (2006) 228–234.

[26] H.Y. Nam, S.M. Kwon, H. Chung, S.-Y. Lee, S.-H. Kwon, H. Jeon, Y. Kim, J.H. Park, J. Kim, S. Her, Y.-K. Oh, I.C. Kwon, K. Kim, S.Y. Jeong, Cellular uptake mechanism and intracellular fate of hydrophobically modified glycol chitosan nanoparticles, J. Control. Release 135 (2009) 259–267.

[27] Mikael J. Pittet, R. Weissleder, Intravital imaging, Cell 147 (2011) 983–991.